STATE OF THE CLIMATE IN 2017

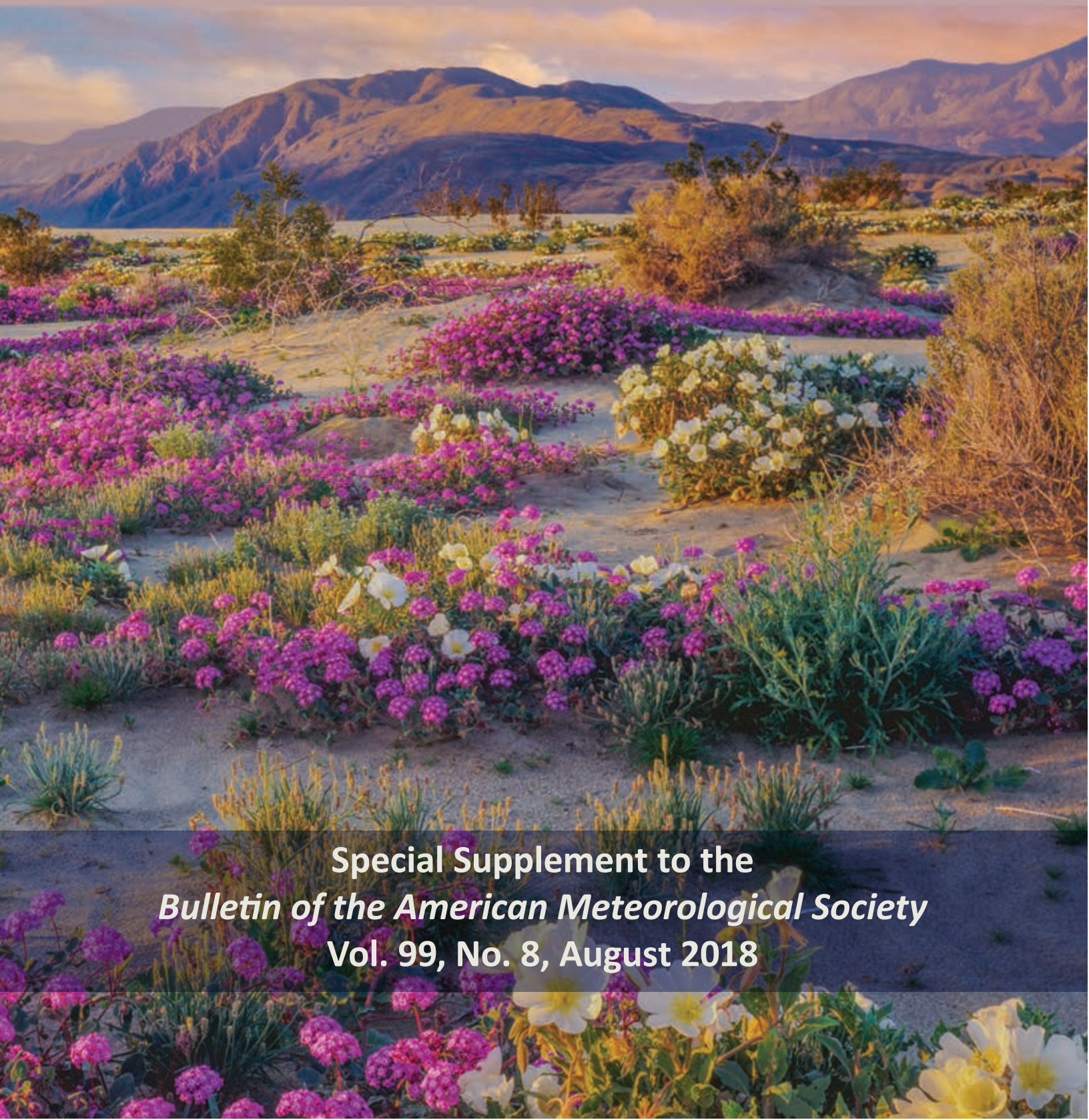

Special Supplement to the
Bulletin of the American Meteorological Society
Vol. 99, No. 8, August 2018

ally integrated in situ 0–700-m OHCA (Fig. 3.6a) all reveal a large increase since 1993, with 2017 being a record high value. A similar pattern is apparent from 700 to 2000 m (Fig. 3.6b). While the trend in globally integrated ocean heat content is modulated by El Niño and is slowed or even reversed after El Niño peaks (Johnson and Birnbaum 2017), it, like globally averaged sea level (see Fig. 3.15a), exhibits a much steadier increase than globally averaged surface temperatures (see Fig. 3.3a). Globally integrated OHCA values vary more both from year-to-year for individual years and from estimate-to-estimate in any given year prior to the achievement of a near-global Argo array around 2005. Causes of differences among estimates are discussed in Johnson et al. (2015).

The rate of heat gain from linear trends fit to each of the six global integral estimates of 0–700 m OHCA from 1993 through 2017 (Fig. 3.6a) range from 0.36 (±0.06) to 0.40 (±0.18) W m^{-2} applied over the surface area of Earth (Table 3.2). Linear trends from 700 to 2000 m over the same time period range from 0.19 (±0.07) to 0.35 (±0.03) W m^{-2}. Trends in the 0–700-m layer all agree within uncertainties, and all but one of the four trends in the 700–2000-m layer do as well. For that layer the PMEL/JPL/JIMAR trend is larger than the others because it assumes the average anomaly in sampled regions applies globally (Lyman and Johnson 2014). For 2000–6000 m, the linear trend is 0.04 (±0.04) W m^{-2} from 1992 to 2010. Summing the three layers (with their slightly different time periods), the full-depth ocean heat gain rate ranges from 0.59 to 0.79 W m^{-2}.

Table 3.2. Trends of ocean heat content increase (in W m^{-2} applied over the 5.1 × 10^{14} m^2 surface area of Earth) from seven different research groups over three depth ranges (see Fig 3.6 for details). For the 0–700-m and 700–2000-m depth ranges, estimates cover 1993–2017, with 5%–95% uncertainties based on the residuals taking their temporal correlation into account when estimating degrees of freedom (Von Storch and Zwiers 1999). The 2000–6000-m depth range estimate, an update of Purkey and Johnson (2010), covers from 1992 to 2010, again with 5%–95% uncertainty.

Research group	Global ocean heat content trends (W m^{-2}) for three depth ranges		
	0–700 m	700–2000 m	2000–6000 m
MRI/JMA	0.36 ± 0.06	0.22 ± 0.06	—
CSIRO/ACE/CRC/IMAS/UTAS	0.40 ± 0.07	—	—
PMEL/JPL/JIMAR	0.40 ± 0.16	0.35 ± 0.03	—
NCEI	0.38 ± 0.07	0.19 ± 0.07	—
Met Office Hadley Centre	0.40 ± 0.18	—	—
ICCES	0.40 ± 0.06	0.19 ± 0.01	—
Purkey and Johnson update	—	—	0.04 ± 0.04

d. Salinity—G. C. Johnson, J. Reagan, J. M. Lyman, T. Boyer, C. Schmid, and R. Locarnini

1) Introduction—G. C. Johnson and J. Reagan

The ocean plays a large role in the global hydrological cycle, with the vast majority of evaporation and precipitation occurring over the oceans (e.g., Schanze et al. 2010). Ocean freshwater storage and transport, and variations thereof, are reflected in salinity patterns and their variations (e.g., Yu 2011). Where evaporation exceeds precipitation, such as in the subtropics, relatively salty surface waters are found. In contrast, where precipitation (and river run off) is greater than evaporation, such as under the ITCZs and in subpolar regions, fresher waters are present. In high latitudes, sea ice formation, advection, and melt also influences SSS (e.g., Petty et al. 2014). Subsurface ocean salinity patterns reflect the surface formation regions of water masses (e.g., Skliris et al. 2014), with fresher tropical waters overlying saltier subtropical waters, which in turn overlay fresher subpolar waters. Below these water masses lie the saltier North Atlantic Deep Water and below that the fresher Antarctic Bottom Water (Johnson 2008). North Atlantic Deep Water temperature and salinity vary over decades (e.g., Yashayaev and Loder 2016), whereas Antarctic Bottom Waters have been freshening in recent decades (e.g., Purkey and Johnson 2013). Salinity changes impact sea level changes (e.g., Durack et al. 2014) as well as the thermohaline circulation (e.g., W. Liu et al. 2017) and have been used to quantify changes in the hydrological cycle (e.g., Skliris et al. 2014).

To investigate interannual changes of subsurface salinity, all available salinity profile data are quality controlled following Boyer et al. (2013) and then used to derive 1° monthly mean gridded salinity anomalies relative to a long-term monthly mean for years 1955–2012 [World Ocean Atlas 2013 version 2 (WOA13v2); Zweng et al. 2013] at standard depths from the surface to 2000 m (Boyer et al. 2013). In recent years, the largest source of salinity profiles is the profiling floats of the Argo program (Riser et al. 2016). These data are a mix of real-time (preliminary) and delayed-mode (scientific quality controlled)

observations. Hence, the estimates presented here could change after all data have been subjected to scientific quality control. The SSS analysis relies on Argo data downloaded in January 2018, with annual maps generated following Johnson and Lyman (2012) as well as monthly maps of bulk (as opposed to skin) SSS data from BASS (Xie et al. 2014). BASS blends in situ SSS data with data from the *Aquarius* (Le Vine et al. 2014; mission ended in June 2015), SMOS (Soil Moisture and Ocean Salinity; Font et al. 2013), and recently SMAP (Soil Moisture Active Passive; Fore et al. 2016) satellite missions. BASS maps can be biased fresh around land (including islands) and at high latitudes. Despite the larger uncertainties of satellite data relative to Argo data, their higher spatial and temporal sampling allows higher spatial and temporal resolution maps than are possible using in situ data alone at present. Salinity is measured as a dimensionless quantity and reported on the 1978 Practical Salinity Scale, or PSS-78 (Fofonoff and Lewis 1979).

2) Sea surface salinity—G. C. Johnson and J. M. Lyman

Sea surface salinity anomalies outside of the tropics are fairly persistent, so 2017 SSS anomalies (Fig. 3.7a, colors) include some extratropical large-scale patterns that largely held from 2004 to 2016 (previous *State of the Climate* reports). Regions around the subtropical salinity maxima are generally salty with respect to WOA13v2, except in the North Pacific, where the salinity maximum is anomalously fresh in 2017. There are fresh anomalies relative to WOA13v2 in much of the high-latitude, low-salinity regions, primarily in portions of the subpolar gyres of the North Pacific and North Atlantic, and to a lesser extent around the Southern Ocean. These multiyear patterns are consistent with an increase in the hydrological cycle (e.g., more evaporation in drier locations and more precipitation in rainy areas) over the ocean, as expected in a warming climate (Rhein et al. 2013). A similar assertion could be made for some of the extratropical 2005–17 trends discussed below.

Tropical sea surface salinity changes from 2016 to 2017 (Fig. 3.7b, colors) are anti-correlated with 2016 to 2017 tendencies in precipitation minus evaporation ($P - E$; see Fig. 3.12b). The freshening in the off-equatorial western tropical Pacific and salinification around the equator in the west and under the ITCZ in the east are all well anti-correlated with $P - E$ tendencies, and associated with the transition from an El Niño that peaked around early 2016 to the neutral or weak La Niña conditions since then. A prominent example of the role of advection by anomalous ocean currents (see Fig. 3.18) in the 2016 to 2017 SSS tendencies is the increase in salinity in the equatorial Indian Ocean. This increase is associated with anomalous eastward currents, consistent with anomalous advection in the presence of mean SSS that decreases from west to east. Other prominent large-scale SSS changes from 2016 to 2017 include freshening in the northeast Pacific, the western tropical Atlantic, and around the equator across much of the Atlantic (Fig. 3.7b).

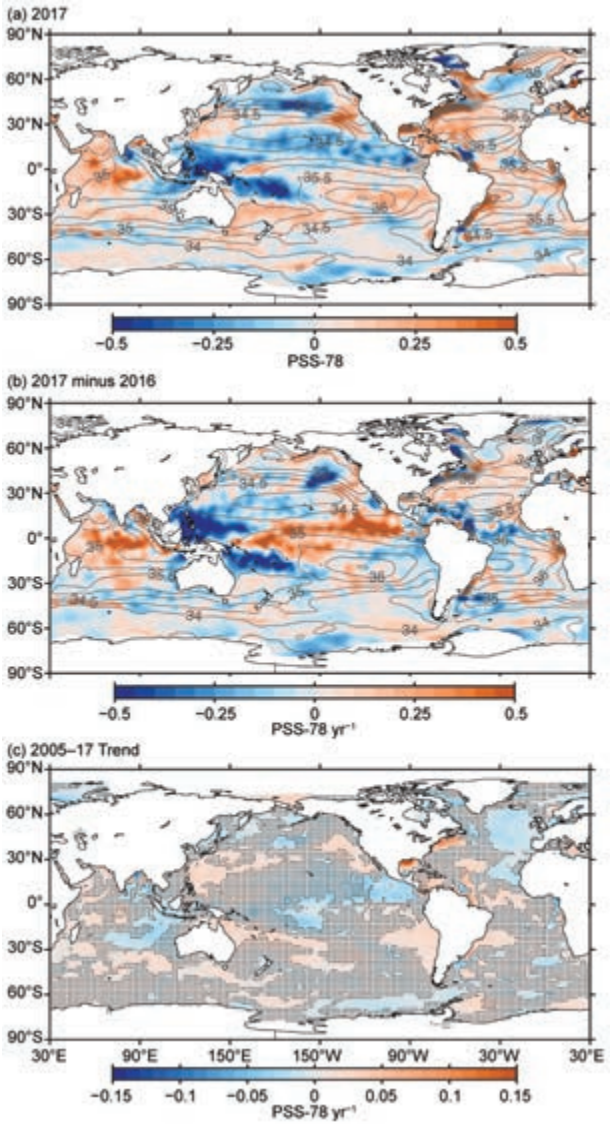

Fig. 3.7. (a) Map of the 2017 annual surface salinity anomaly (colors, PSS-78) with respect to monthly climatological 1955–2012 salinity fields from WOA13v2 [yearly average (gray contours at 0.5 intervals), PSS-78]. (b) Difference of 2017 and 2016 surface salinity maps (colors, PSS-78 yr^{-1}). White ocean areas are too data-poor (retaining < 80% of a large-scale signal) to map. (c) Map of local linear trends estimated from annual surface salinity anomalies for 2005–17 (colors, PSS-78 yr^{-1}). Areas with statistically insignificant trends are stippled. All maps are made using Argo data.

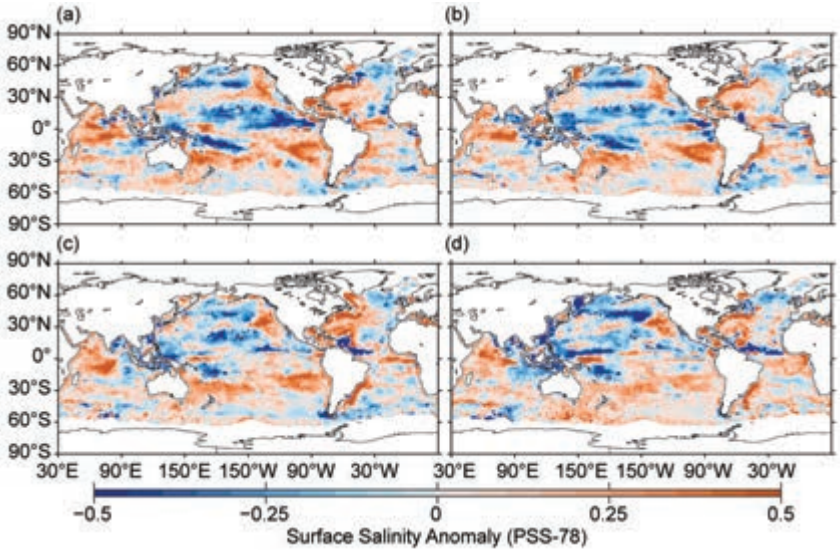

Fig. 3.8. Seasonal maps of SSS anomalies (colors) from monthly blended maps of satellite and in situ salinity data (BASS; Xie et al. 2014) relative to monthly climatological 1955–2012 salinity fields from WOA13v2 for (a) Dec–Feb 2016/17, (b) Mar–May 2017, (c) Jun–Aug 2017, and (d) Sep–Nov 2017. Areas with maximum monthly errors exceeding 10 PSS-78 are left white.

Strong seasonal variations of BASS (Xie et al. 2014) SSS anomalies (Fig. 3.8) are evident near the Amazon and Orinoco River plumes. While there is almost no fresh signal in December–February, a strong fresh anomaly extends north of the river mouths in March–May and grows to the north and extends eastward in June–August, with a strong fresh anomaly extending across much of the northern equatorial Atlantic in September–November. Other factors, including stronger-than-usual precipitation in the region (see Fig. 3.12), likely contributed to the fresh anomaly as well. In the tropical Pacific, fresh anomalies in the eastern Pacific warm pool diminished throughout the year while the western Pacific warm pool freshened, again consistent with the shift of precipitation to the western tropical Pacific after the 2015/16 El Niño and persistence of neutral and La Niña conditions throughout 2017.

Sea surface salinity trends for 2005–17 (Fig. 3.7c) are estimated by local linear fits to annual average SSS maps from Argo data. (The starting year is 2005 because that is when Argo coverage became near-global.) Regions with statistically significant increasing salinity trends are found near the subtropical salinity maxima in all the ocean basins, although the eastern subtropical North Atlantic is freshening, even near the salinity maximum. In the higher latitudes and the tropics, where mean salinity values are lower, there are some regions where the trend is toward freshening. In high latitudes, these freshening regions include the subpolar North Atlantic and North Pacific, as well as patches in the Pacific and Atlantic sectors of the Southern Ocean. In the tropics, they include the central Pacific, at the eastern edge of the western fresh pool, and in the warm fresh pool of the northeastern equatorial Pacific. There are also freshening trends in the already fresh Bay of Bengal, and a large patch west of Indonesia and Australia that has been present since at least 2009 (see previous *State of the Climate* reports). The regions to the northwest of the Gulf Stream and in the northern Gulf of Mexico are also trending strongly saltier, as well as warmer (Section 3c).

3) Subsurface salinity—J. Reagan, T. Boyer, C. Schmid, and R. Locarnini

For the first time in the past decade, nearly all 2017 Atlantic Ocean basin-average monthly salinity anomalies were positive from 0 to 1500 m (Fig. 3.9a). The year 2017 continued the same Atlantic salinity anomaly pattern that has been evident since 2008 with strong positive (> 0.05) near-surface salinity anomalies that weaken with depth (~0.005 at 700 m) (Fig. 3.9a). Salinity increased at nearly all depths within 0–1500 m from 2016 to 2017 (Fig. 3.9b) with the highest increase between 100 and 125 m (~0.017).

The 2017 Pacific Ocean basin-average salinity anomalies continued the same pattern that began in mid-2014 with fresh anomalies from 0 to 75 m, salty anomalies from 100 to 200 m, and fresh anomalies from 200 to 600 m (Fig. 3.9c). This marks the third straight year (2015–17) in which the upper ~75 m of the Pacific Ocean has been fresher than the long-term average. Previously, this layer had been saltier than the long-term average for five straight years (2009–13; Fig. 3.9c). These basin-average multiyear near-surface salinity shifts may be related to in-phase transitions of both ENSO and the PDO and their associated precipitation (Lau and Yang 2002) and equatorial wind stress/Ekman upwelling changes (Wang et al. 2015). From 2016 to 2017 the upper 125 m of the Pacific became fresher (max of ~ −0.018 at 0 m), while the 150–400-m layer became saltier (max of ~0.013 at 200 m; Fig. 3.9d).

From mid-2016 through 2017 the upper 200 m of the Indian Ocean became very salty (> 0.05 near the surface) when compared to the long-term mean

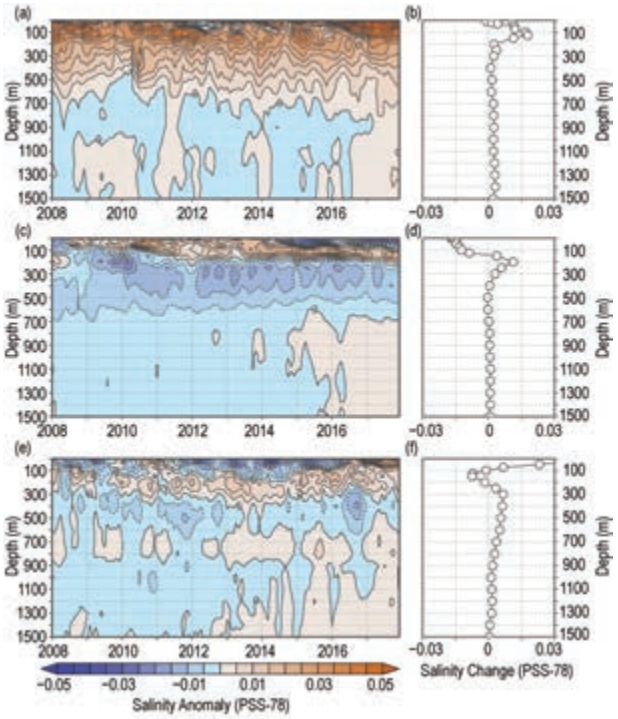

Fig. 3.9. Average monthly salinity anomalies (PSS-78) relative to the long-term WOA13v2 monthly salinity climatology for years 1955–2012 (Zweng et al. 2013) from 0 to 1500 m for the (a) Atlantic for 2008–17 and (b) the change from 2016 to 2017; (c) Pacific for 2008–17 and (d) the change from 2016 to 2017; (e) Indian for 2008–17 and (f) the change from 2016 to 2017. Data were smoothed using a 3-month running mean.

(Fig. 3.9e). Much of the surface of the Indian Ocean experienced salty anomalies (Fig. 3.7a) that were not driven directly by changes in $P-E$ (see Fig. 3.12a) but were due to anomalous ocean currents (see Fig. 3.18a and Section 3d2). Unsurprisingly, there was a large (~0.05 at 0 m; Fig. 3.9f) salinification of the near-surface from 0 to 100 m between 2016 and 2017, with freshening from 100 to 200 m, and salinification from 200 to 1000 m (Fig. 3.9f).

Most of the large (> |0.09|) zonally averaged salinity changes from 2016 to 2017 in the Atlantic occurred in the North Atlantic (Fig. 3.10a). There was freshening in the upper 50 m from 0° to 20°N, with maximum freshening (< −0.12) at ~10 m depth. This is in contrast to the salinification that was observed in this region between 2015 and 2016 (see Fig. 3.10a in Reagan et al. 2017). The freshwater discharge from the Amazon and Orinoco Rivers are likely the source of this freshening (Figs. 3.7b and 3.8a–d) with a stronger 2017 North Brazil Current (when compared to 2016) from March through August (see Figs. 3.19b,c) helping advect the freshwater river discharge farther to the north and northwest. Increased $P-E$ (see Fig. 3.12a) over the Atlantic ITCZ may have also played a role in the freshening over this area. North of this freshening, there was salinification (> 0.03) between 2016 and 2017 from 20° to 52°N, which expanded and deepened from the surface to 100 m at 20°N to 400 m at 50°N with maximum salinification (> 0.09) occurring at 50 m at 47.5°N.

The zonally averaged Pacific salinity changes from 2016 to 2017 are primarily concentrated in the upper 150 m (Fig. 3.10b). Near-surface (0–50 m) freshening (< −0.03) at 22°S extends equatorward and deepens to 150 m at 8°S with maximum freshening (< −0.12) at the surface near 15°S. This is a reversal of the salinification that took place from 2015 to 2016 in this area, and it is likely due to the transition from the strong El Niño in early 2016 to the neutral and weak La Niña conditions that dominated 2017 and its associated precipitation tendencies from 2016 to

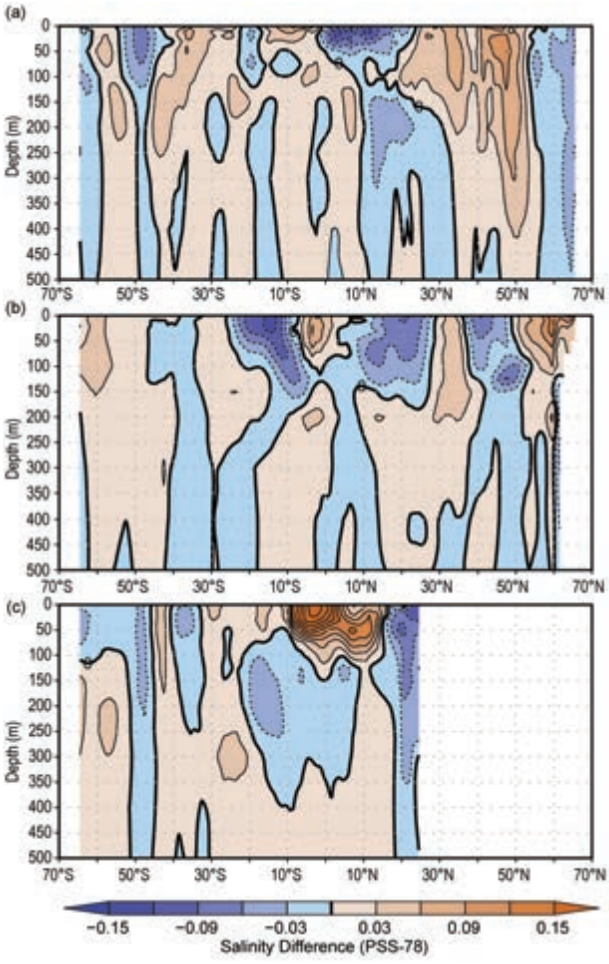

Fig. 3.10. Difference between the 2017 and 2016 zonal average monthly salinity anomalies (PSS-78) relative to the long-term WOA13v2 monthly salinity climatology for 1955–2012 (Zweng et al. 2013) from 0 to 500 m for the (a) Atlantic, (b) Pacific, and (c) Indian Ocean basins. Contours are multiples of ±0.03 with a bold 0 contour.

2017 (see Fig. 3.12d). Near the equator, salinity increased between 2016 and 2017, likely due to the aforementioned ENSO transition and upwelling of higher salinity water caused by increased zonal wind stress from 2016 to 2017 (see Fig. 3.13b). Farther north there was freshening (< −0.03) from 10° to 27°N reaching a depth of ~140 m and freshening (< −0.03) between 38° and 50°N from 0 to 150 m. Finally, there was salinification (> 0.03) between 50° and 60°N in the upper 100 m.

The largest changes in zonally averaged salinity between 2016 and 2017 in the Indian Ocean occurred in the upper 100 m between 10°S and 15°N (Fig. 3.10c). In this region, there was broad-scale salinification (> 0.03) with large increases in salinity (> 0.20) in the upper 50 m between 10°S and the equator. As was discussed previously in this section, this salinification was primarily due to the advection of salty water via 2017 anomalous ocean currents (see Fig. 3.18a). Freshening (< −0.03) from 2016 to 2017 from 17° to 24°N extends down to 350 m and is primarily caused by the near-coast freshening along India's west coast (Fig. 3.7b).

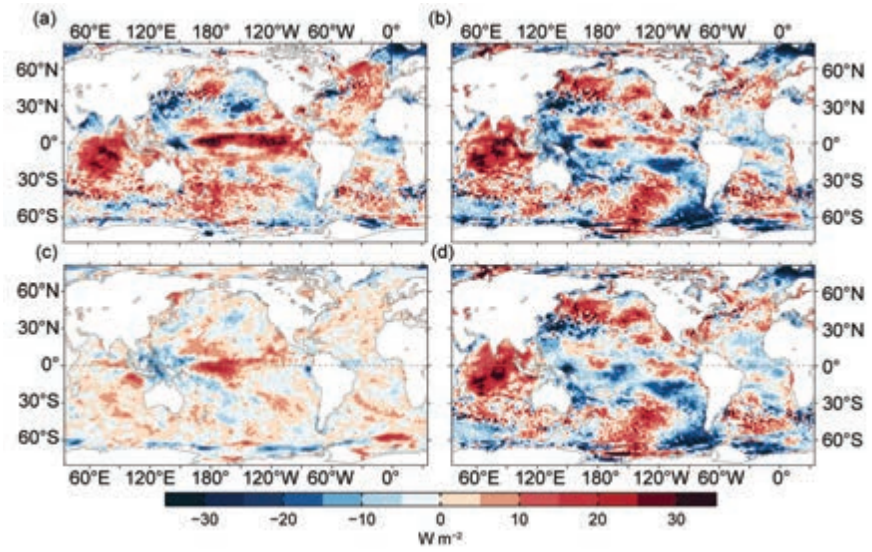

Fig. 3.11. (a) Surface heat flux (Q_{net}) anomalies (W m^{-2}) for 2017 relative to the 2010–14 mean. Positive values denote ocean heat gain. 2017 minus 2016 difference for (b) Q_{net}, (c) surface radiation (SW+LW), and (d) turbulent heat fluxes (LH+SH), respectively. Positive differences denote more ocean heat gain in 2017 than in 2016. LH+SH are produced by the OAFlux high-resolution (HR) satellite-based analysis, and SW+LW by the NASA FLASHFlux project.

e. *Global ocean heat, freshwater, and momentum fluxes*—L. Yu, X. Jin, S. Kato, N. G. Loeb, P. W. Stackhouse, R. A. Weller, and A. C. Wilber

The ocean and the atmosphere communicate via interfacial exchanges of heat, freshwater, and momentum. These air–sea fluxes are the primary mechanisms for keeping the global climate system nearly balanced with the incoming insolation at Earth's surface. Most of the shortwave radiation (SW) absorbed by the ocean's surface is vented into the atmosphere by three processes: longwave radiation (LW), turbulent heat loss by evaporation (latent heat flux, or LH), and conduction (sensible heat flux, or SH). The residual heat is stored in the ocean and transported by ocean circulation, forced primarily by the momentum transferred to

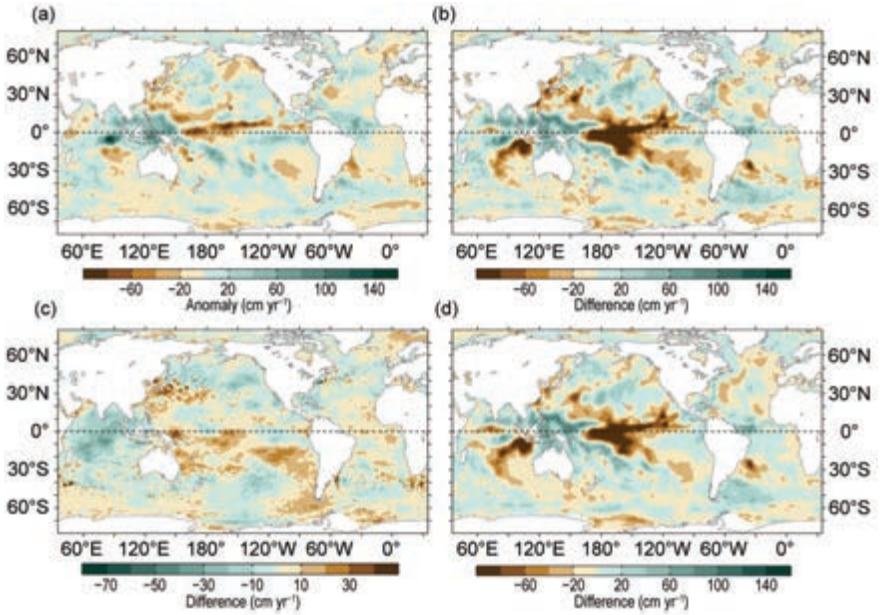

Fig. 3.12. (a) Surface freshwater (*P*–*E*) flux anomalies (cm yr^{-1}) for 2017 relative to a 1988–2014 climatology. 2017 minus 2016 tendencies for (b) *P*–*E*, (c) evaporation (*E*), and (d) precipitation (*P*). Green colors denote anomalous ocean moisture gain and browns denote loss, consistent with the reversal of the color scheme in (c). *P* is computed from the GPCP version 2.3 product, and *E* from OAFlux-HR satellite-based analysis.